Draft version October 2, 2025
Typeset using LaTeX **twocolumn** style in AASTeX631

Hot Jupiters' Isolation Is Not Unique to High-Eccentricity Tidal Migration

Brandon T. Radzom [1], Songhu Wang [1], Bonan Pu [2], Hareesh Gautham Bhaskar,[1] Malena Rice [3]
(AAS Journals Data Editors)

[1] *Department of Astronomy, Indiana University, 727 East 3rd Street, Bloomington, IN 47405-7105, USA*
[2] *Independent Researcher*
[3] *Department of Astronomy, Yale University, 219 Prospect Street, New Haven, CT 06511, USA*

ABSTRACT

Despite decades of effort, the origins of short-period gas giants remain contested. Previous searches for nearby planetary companions to hot Jupiters ($P < 10$ days) have indicated that the vast majority of these close-in giants are isolated, in stark contrast to their wider-orbiting counterparts known as warm Jupiters, which appear to routinely host nearby companions. This dichotomy in companionship has been interpreted as evidence of disparate formation histories, with the origins of hot Jupiters being more dynamically violent, involving some form of high-eccentricity tidal migration. In this study, however, we adopt a unified quiescent framework for both populations wherein they emerge from the protoplanetary disk as the sole giant planet within a compact multi-super-Earth system. We use long-term numerical simulations to show that post-disk dynamical evolution will naturally result in an observed preferential isolation for hot Jupiters. Specifically, their companions achieve significantly larger period ratios and mutual inclinations, rendering them more difficult to detect — especially via transits and transit timing variations. Additionally, we find that this paradigm can explain the tendency for longer-period hot Jupiters to host nearby companions on co-planar interior orbits, as well as the existence of ultra-short-period planets in short-period giant systems (when tidal effects are considered). A generic prediction of this model, which is readily testable with modern high-precision Doppler velocity measurements, is that hot Jupiters should commonly host close-in ($P \lesssim 50$ days), mutually inclined companions.

1. INTRODUCTION

The longest-standing mystery in exoplanet astronomy pertains to the origins of short-period Jovian-class planets such as hot Jupiters (as comprehensively reviewed by Dawson & Johnson 2018). Proposed theories to explain the existence of these gas giants can be categorized as either dynamically quiescent or violent. Mechanisms labeled as "dynamically quiescent" include disk migration, wherein the giant forms in the outer regions before moving inward through interactions with their disk (Goldreich & Tremaine 1979; Lin & Papaloizou 1986; Lin et al. 1996), and in situ formation, wherein the giant forms at or proximate to its current orbit (Lee et al. 2014; Boley et al. 2016; Batygin et al. 2016; Bailey & Batygin 2018). The "dynamically violent" mechanisms encompass a variety of high-eccentricity tidal migration pathways which can be triggered by planet-planet scattering (Rasio & Ford 1996; Chatterjee et al. 2008), Lidov-Kozai cycling (Wu & Murray 2003; Fabrycky & Tremaine 2007; Naoz 2016), or secular chaos (Wu & Lithwick 2011; Lithwick & Wu 2014; Hamers et al. 2017).

Independently, these formation and evolution channels can each explain only a subset of the known observational characteristics of short-period gas giants (Dawson & Johnson 2018). One such property, currently challenging each origin model individually, is the observed preferential isolation of hot Jupiters ($P < 10$ days) relative to their wider-orbiting (10 days $\leqslant P \lesssim 300$ days) giant counterparts, known as warm Jupiters (see Spalding & Batygin 2017 for an exception). Specifically, the earliest population studies demonstrated that hot Jupiters were effectively devoid of any nearby low-mass planetary companions, with less than 1% hosting a nearby co-transiting neighbor, while more than half of

Corresponding author: Brandon T. Radzom
bradzom@iu.edu

warm Jupiters had such companions (e.g., Steffen et al. 2012; Huang et al. 2016). This stark companionship dichotomy served as strong evidence of dichotomous histories for these two populations of short-period giants, with quiescent mechanisms being dominant for warm Jupiters and violent high-eccentricity migration, which is capable of clearing out any close-in companions (Mustill et al. 2015), producing most hot Jupiters. However, the latest results from TESS and transit timing variation searches (TTVs) for nearby companions firmly establish that a non-negligible fraction ($\gtrsim$ 7–12%) of hot Jupiters are not lonely (Hord et al. 2021; Wu et al. 2023), and hence may have shared origins with warm Jupiters.

In this work, we investigate whether a unified dynamically quiescent framework for both hot Jupiters and warm Jupiters can explain their observed companionship dichotomy. Specifically, we use long-term N-body simulations of short-period giants in compact multi-planet systems to demonstrate that, through gravitational interactions alone, hot Jupiters naturally self-isolate relative to warm Jupiters. We find that dynamical evolution in such systems drives the companions of hot Jupiters to become significantly more sparsely spaced, more mutually inclined, and ultimately more difficult to detect compared to warm Jupiters. Further, consistent with observations, this model predicts that the shortest-period hot Jupiters appear the most isolated, while those at wider periods of P = 4–10 days can host nearby, inner companions on co-planar orbits. Additionally, we find that, when planetary tides are taken into account, a substantial subset of surviving inner companions to both hot Jupiters and warm Jupiters wind up on ultra-short-period orbits, as is also seen observationally. While the underlying formation mechanism for short-period giants in such compact systems is unclear, our results show that the observed preferential isolation of hot Jupiters is not a feature that is unique to violent origins such as high-eccentricity migration, providing important context for interpreting companionship studies.

2. SIMULATION SET-UP

Overview. We generate 360 primordial peas-in-a-pod planetary systems that resemble more compact, higher-multiplicity versions of *Kepler* multiple-planet systems, which are packed near the boundary of Hill stability (Pu & Wu 2015; Volk & Gladman 2015). Such a set-up is well-motivated by evidence showing that current-day *Kepler* multi-planet systems may have undergone significant dynamical sculpting in the past, originating from pristine systems with more planets in tighter configurations (e.g., Izidoro et al. 2017; Zink et al. 2019; Izidoro et al. 2021). Particularly, each of our systems begins with twelve nearly uniformly and closely spaced super-Earths with similar masses orbiting a solar-mass star (similar to the set-up used in Goldberg & Batygin 2022). Before integration, we select one super-Earth in each system to have a wider spacing with its nearest neighbors, and replace this planet with a Jupiter-mass (1 M_J) giant, which will trigger dynamical instability in the absence of eccentricity damping from the disk (Ward 1997; Chatterjee et al. 2008).

Planetary Mass & Radius. We assign planetary masses according to a Gaussian distribution centered on 6 $M_\oplus$ (Wu et al. 2019; consistent with typical masses in *Kepler* multi-planet systems) with $\sigma_m = 20\% \times 6\,M_\oplus = 1.2\,M_\oplus$ and within the range $1\,M_\oplus - 10\,M_\oplus$. We determine planetary radii from their masses using the mass-radius relation for rocky, volatile-poor bodies described in Equation 1 of Otegi et al. (2020). We note that our results do not sensitively depend on the exact masses (nor radii) of our small planets, as they are much less massive than our giants.

Spacing. To generate probable progenitors to *Kepler*-like peas-in-a-pod systems, we employ an adaptation similar to the Equal Mutual Separation (EMS) scheme (e.g., Chambers et al. 1996; Zhou et al. 2007). Specifically, we set the planet spacing parameter to $K = 10$, which is not only consistent with expectations from planet formation (e.g., Kokubo & Ida 1998) but also corresponds to the critical boundary for instability defined by Funk et al. (2010) for $N \geqslant 8$ systems and the compact tail of the expected intrinsic distribution for observed *Kepler* multi-planet systems (Pu & Wu 2015). The spacing parameter plays an important role in setting the dynamical stability timescale for EMS systems (Obertas et al. 2017) and is defined as

$$K = \frac{a_j - a_{j-1}}{r_{H,\mathrm{mut}}} \tag{1}$$

where a_j and a_{j-1} are the semi-major axes of the j^{th} and $(j-1)^{th}$ planets from the star, and $r_{H,\mathrm{mut}}$ is their mutual Hill radius

$$r_{H,\mathrm{mut}} = \frac{a_j + a_{j-1}}{2}\left(\frac{m_j + m_{j-1}}{3M_*}\right)^{1/3} \tag{2}$$

where m_j and m_{j-1} are the masses of the j^{th} and $(j-1)^{th}$ planets, respectively, and M_* is the mass of the central star.

Since the planetary masses within each of our simulated near-EMS systems are similar, the period ratios P_{j+1}/P_j between adjacent planets are also nearly identical, with a characteristic value of 1.43 — intermediate of the 7:5 and 3:2 mean motion resonances (MMRs).

To sample a more continuous distribution for the orbital period of our giants, we also vary the period of the innermost planet by drawing from a half-normal distribution with $\mu_P = 3$ days (near the observed inner edge of multi-planet systems; Mulders et al. 2018) and $\sigma_P = 10\% \times \mu_P = 0.3$ days. The minimum possible innermost period is thus set at μ_P, and we impose a maximum value for this period at 4 days. Given our spacing scheme and selected multiplicity ($N = 12$), our simulations probe a period range of 3 days $\leqslant P \lesssim 300$ days, which is consistent with the finite range identified for observed peas-in-a-pod systems (Millholland et al. 2022).

Eccentricity & Inclination. In agreement with known *Kepler* compact multi-planet systems, we ensure that the planets in our systems begin on orbits that are nearly circular and co-planar (Xie et al. 2016; Zhu et al. 2018; Millholland et al. 2021). We limit the orbital eccentricities e of each planet to be less than the orbit-crossing value e_c of each system, computed as

$$e_c \approx \frac{1}{2}\left[\left(\frac{a_{\rm outer}}{a_{\rm inner}}\right)^{1/(N-1)} - 1\right] \quad (3)$$

where N is the total number of planets in the system (always initially 12), and $a_{\rm outer}$ and $a_{\rm inner}$ are the outermost and innermost semi-major axes of each planetary system, respectively. The typical value expected for each system in our fiducial simulations is $e_c = 0.15$. With this upper limit established, we pull eccentricities for each planet from a Rayleigh distribution with $\sigma_e = 10\% \times e_c = 0.015$. We draw orbital inclinations from a Rayleigh distribution as well with standard deviation $\sigma_\theta = \sigma_e/2 \times (180^\circ/\pi)$, and impose an upper limit of 3°.

Oscillating Angles. The values for the longitude of the ascending node (Ω), as well as the sum of the argument of periapsis (ω) and the true anomaly (M), are chosen randomly from $[0, 2\pi]$.

Giant Planet Insertion. Once our peas-in-a-pod super-Earths are in place, we select one planet per system to become a giant. While the details of the disk properties and physical mechanisms required for the planet to undergo runaway accretion are uncertain, we attempt to account for this uncertainty by increasing the mutual spacing of the "proto-giant" with its nearest neighbors by a random amount. Specifically, we determine this spacing enhancement δK by pulling from a Gaussian distribution with a large standard deviation $\sigma_K = 10$, such that the typical K (68% confidence interval) for this planet is double its initial value. An upper limit is imposed on δK such that the final modified spacing, assuming a 1 M_J giant, cannot exceed the fiducial $K = 10$ spacing. This local spacing buffer is consistent with a range of possible scenarios wherein the proto-giant super-Earth core opens a partial gap in the disk (Rafikov 2002; Paardekooper & Mellema 2004, 2006), potentially accreting materials from its neighboring planets' reservoirs.

Once the chosen super-Earth's spacing is enhanced, we boost its mass to 1 M_J and radius to 1 R_J. We sample each of the twelve possible spots for giant insertion in each system (from $j = 1$–12) 30 times. Since every super-Earth progenitor system is generated from scratch, we end up with $12 \times 30 = 360$ unique compact multi-planet systems in total, each containing one giant. Replacing a super-Earth with a Jovian-class planet reduces the typical minimum K value in our systems, of which the instability timescale is a strong function (Wu et al. 2019), to lie in the range 3.33–6.67 (i.e., the 68% confidence interval for the spacing between the giant and its nearest companion). Therefore, while most minimum spacings sit safely above the $K = 3.5$ limit for two-body Hill instability (Gladman 1993), many also fall below the instability limit needed for high-multiplicity ($N > 3$) systems (Funk et al. 2010; Obertas et al. 2017), ensuring dynamical disruption ensues in our multi-planet systems.

Integration. We utilize the hybrid integrator `TRACE` in `REBOUND` (Rein & Liu 2012; Rein & Spiegel 2015; Lu et al. 2024) to run the N-body integrations for each of our 360 systems. Since the giant planet is the dominant body in each system, we integrate to a fixed number of giant orbits ($P_{\rm giant}$), rather than a fixed time, to ensure that each system reaches roughly the same dynamical age. In order to balance computational cost and achieving long-term stability, we elect to integrate each system to 10^9 giant orbits (i.e., $10^9 P_{\rm giant}$). Direct physical collisions are enabled and resolved with the conservation of mass and momentum. Planets are considered ejected and are removed from the system once their distance from the central star is greater than 250 AU. Commentary on conserved quantities and other relevant integration details is provided in Appendix 8.

3. FIDUCIAL SIMULATION RESULTS

3.1. *System-Wide Isolation for Hot Jupiters*

For both hot Jupiters ($P < 10$ days) and warm Jupiters ($P \geqslant 10$ days), we find that at least one planetary companion is retained and calculate a mean companion multiplicity of ~ 3.5. To quantify the relative degree of isolation for both giant populations, we compute their period ratios with each remaining companion, finding that hot Jupiters boast a $\approx 60\%$ larger median value ($10.60^{+3.46}_{-0.44}$) compared to warm Jupiters ($6.45^{+0.47}_{-0.12}$), with significantly larger dispersion. In Figure 1, we

plot the cumulative distribution function (CDF) of these period ratios for hot Jupiters and warm Jupiters separately, demonstrating a clear dichotomy between the two giant populations.

To better quantify the strength of this dichotomy, we perform a two-sample Anderson-Darling (AD) test (Darling 1957), which is similar in nature to the well-known Kolmogorov–Smirnov (KS) test (Kolmogorov & Morrison 1950; Smirnov 1939), but has been demonstrated to have superior statistical power (Scholz & Stephens 1987; Hou et al. 2009; Egmann & Cousineau 2011). To ensure the precision in our computed p-value lies well below commonly-adopted significance thresholds (e.g., 0.05 or 0.005; Wasserstein & Lazar 2016), we utilize the permutation method (implemented in `scipy.stats.anderson_ksamp`) with 10,000 re-samplings rather than rely on interpolation of a grid of pre-calculated values (Scholz & Stephens 1987; Feigelson & Babu 2013), which allows us to measure down to $p = 10^{-4}$. The null hypothesis we test is that the underlying distributions of companion period ratios are the same for our simulated hot Jupiters (327 companions) and warm Jupiters (933 companions). We find this null hypothesis is firmly rejected by the AD test, and compute a resulting p-value at our precision floor of $p \leqslant 10^{-4}$.

The inflated period ratios in hot Jupiter systems imply dynamically hotter evolution compared to warm Jupiter systems. Indeed, we find that the companions of hot Jupiters also become more mutually inclined, boasting a median mutual inclination[1] of $\mathcal{I}_{\rm mut} = 5.14^{+0.47}_{-0.21}{}^{\circ}$ — nearly 60% higher, and also with greater dispersion (7.49°), than that of warm Jupiters' ($\mathcal{I}_{\rm mut} = 3.30^{+0.16}_{-0.07}{}^{\circ}$, dispersion: 5.18°). The distributions of companion mutual inclinations for both giant populations are also statistically distinct; our AD test yields a p-value of $\leqslant 10^{-4}$. Therefore, the companions of hot Jupiters tend to be both more widely spaced and mutually inclined compared to those of warm Jupiters. We summarize these results in the top portion of Table 1.

Table 1. Summary of Key Companionship Results for Fiducial Simulations

Metric[a]	Hot Jupiters	Warm Jupiters	p[b]
Conventional boundary ($P = 10$ days)			
All companions			
Median P_{j+1}/P_j	$10.60^{+3.46}_{-0.44}$	$6.45^{+0.47}_{-0.12}$	10^{-4}
Median $\mathcal{I}_{\rm mut}$ (°)	$5.14^{+0.47}_{-0.21}$	$3.30^{+0.16}_{-0.07}$	10^{-4}
Nearest companions			
Median P_{j+1}/P_j	$2.76^{+0.45}_{-0.07}$	$3.16^{+0.09}_{-0.06}$	10^{-3}
Median $\mathcal{I}_{\rm mut}$ (°)	$3.26^{+0.51}_{-0.24}$	$2.86^{+0.19}_{-0.12}$	0.1947
Max isolation ($P = 7.5$ days)			
All companions			
Median P_{j+1}/P_j	$14.55^{+4.05}_{-0.76}$	$6.46^{+0.52}_{-0.11}$	10^{-4}
Median $\mathcal{I}_{\rm mut}$ (°)	$5.16^{+0.47}_{-0.24}$	$3.43^{+0.16}_{-0.07}$	10^{-4}
Nearest companions			
Median P_{j+1}/P_j	$3.30^{+0.79}_{-0.16}$	$3.08^{+0.08}_{-0.05}$	10^{-4}
Median $\mathcal{I}_{\rm mut}$ (°)	$3.92^{+0.61}_{-0.35}$	$2.76^{+0.17}_{-0.11}$	0.0011

[a] Reported uncertainties are standard errors calculated using the 84th and 16th percentile values, weighted by the number of companions.

[b] p-value obtained via a two-sample AD test of the metric.

3.2. *Architectural Dichotomy*

To understand how these system-wide companionship trends translate to scales local to our giants, we repeat the above analysis restricted to only their closest neighbors, i.e., the companions with the minimum period ratio in their system (94 companions for hot Jupiters, 266 for warm Jupiters). We also tabulate these results in Table 1; while we find that hot Jupiters' period ratios again show more scatter, their median value is now comparable to warm Jupiters'. Regardless, the null hypothesis is still rejected by our AD test ($p = 10^{-3}$). Regarding their mutual inclinations, there are no longer any strong indications of statistically distinct distributions: the null hypothesis cannot be rejected ($p = 0.1947$), and hot Jupiters' companions show only marginally inflated median inclinations (and a modestly higher dispersion of 4.68° compared to 3.65°). Figure 2, which displays the distribution of minimum period ratios and their relative directions as a function of giant orbital period, provides important context. Namely, we see that the nearest companions to the shortest-period ($P \lesssim 7$ days) hot Jupiters may end up on either very nearby ($P_{j+1}/P_j < 3$) or isolated orbits ($P_{j+1}/P_j > 6$), taking on a wide range of period ratios, while most warm Jupiters' nearest companions reside on nearby orbits. Further, there

[1] To calculate mutual inclinations, we first compute the complex inclinations $\mathcal{I}$ of the companion and the giant as $\mathcal{I} = \theta e^{i\Omega}$ where i is the imaginary unit, and θ and Ω are the orbital inclination and longitude of the ascending node, respectively. Then, we calculate the absolute difference between these complex values to get the mutual inclination at the final timestep. Finally, to account for potentially significant inclination oscillations, we compute these inclinations over 500 orbits and adopt the root-mean-square as the mutual inclination $\mathcal{I}_{\rm mut}$.

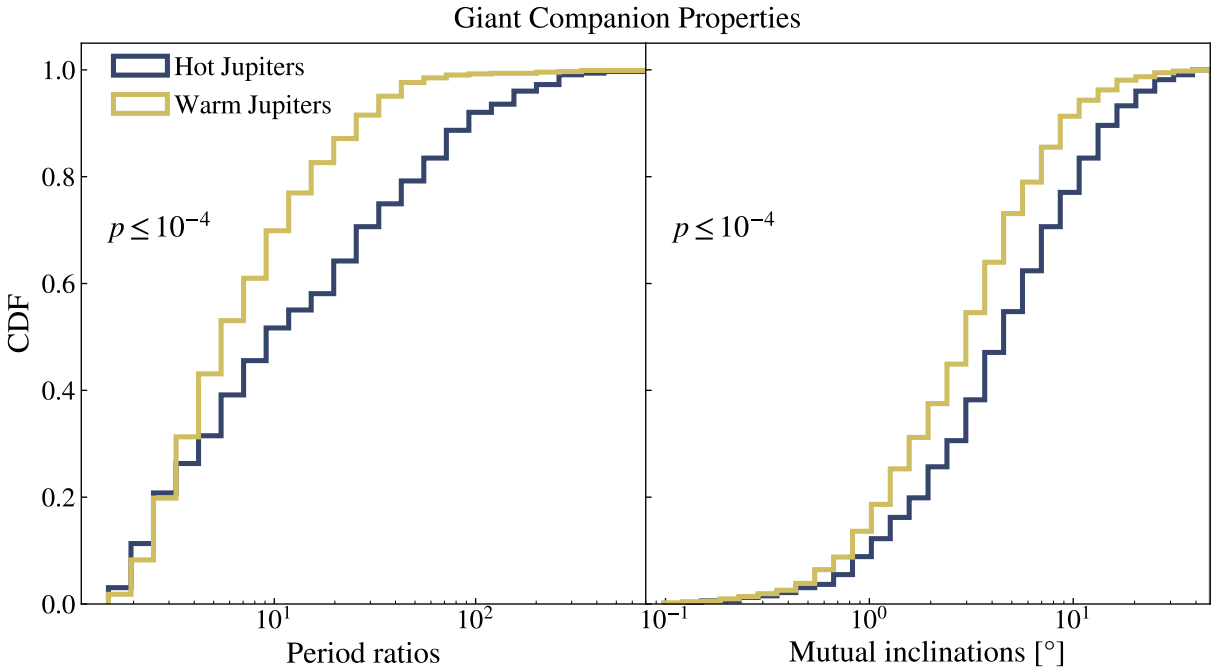

Figure 1. CDFs for the final period ratios (left) and mutual inclinations (right) of our giant planets and their neighboring super-Earth companions, plotted separately for hot Jupiter systems (blue) and warm Jupiter systems (yellow). The p-values obtained from our AD tests on the hot and warm Jupiter distributions are displayed center-left in both panels. As evidenced in the plot and our computed p-values, hot Jupiters and warm Jupiters naturally produce companions with statistically distinct properties, with hot Jupiters' companions exhibiting higher period ratios and mutual inclinations.

is a rapid evolution from isolated to exceptionally compact configurations at $P \approx 7$ days, beyond which even hot Jupiters commonly host nearby interior companions. This transition is indicative of a stronger companionship dichotomy defined across a slightly shorter orbital period than the conventional $P = 10$ days hot Jupiter-warm Jupiter boundary.

3.3. *The Maximum Isolation Boundary*

Motivated by the empirical transition from highly-scattered, larger period ratios to tightly-clustered, small period ratios around $P \approx 7$ days apparent in Figure 2, we attempt to quantitatively identify an orbital period boundary driven by our simulation data that better separates isolated "hot Jupiters" from non-isolated "warm Jupiters". Specifically, we numerically sort the orbital periods of our giant planets and begin by creating a bin containing the 30 shortest-period giants, which we consider as canonical "hot Jupiters" (centered on $P = 3.27$ days and bounded by $P = 2.83$ days and $P = 3.71$ days). We then compute the 14^{th}, 50^{th}, and 86^{th} percentiles of the period ratio distribution for their nearest companions, and measure the sample's deviation from isolation by calculating the distribution's z-score relative to our adopted isolation period ratio threshold of $P_{j+1}/P_j = 6$. The bin is then translated forward in period space to absorb the next giant in our sorted list (and drop the first), and this process is iteratively repeated until the end of the list is reached. Adopting a fixed bin size of 30 systems helps ensure our z-scores are statistically robust and avoids biases and uncharacterized sources of uncertainty that would be introduced by unequal bin sizes (e.g., see Goyal & Wang 2025).

We plot the resultant z-scores of this moving-bin test in Figure 3, finding that our giants remain significantly isolated (at or above the 3σ level) out to $P = 7.5 \pm 1.1$ days. Adopting this period cut as an alternate hot Jupiter-warm Jupiter boundary, we re-compute all companionship metrics and summarize our results in Table 1. Broadly, we find that this boundary of maximum isolation produces an enhanced dichotomy; the companions to "hot Jupiters" exhibit wider period ratios and modestly enhanced mutual inclinations compared to the conventional 10-day cut. Critically, all AD tests now yield $p \leqslant 0.005$, demonstrating that the period ratio and mutual inclination distributions for all companions, even the closest neighbors, are statistically distinct assuming this boundary.

While the conventional $P = 10$ days boundary is arbitrary, we note that the purpose of this exercise is not to identify an alternate cut for the observed hot Jupiter population but instead to characterize the maximal com-

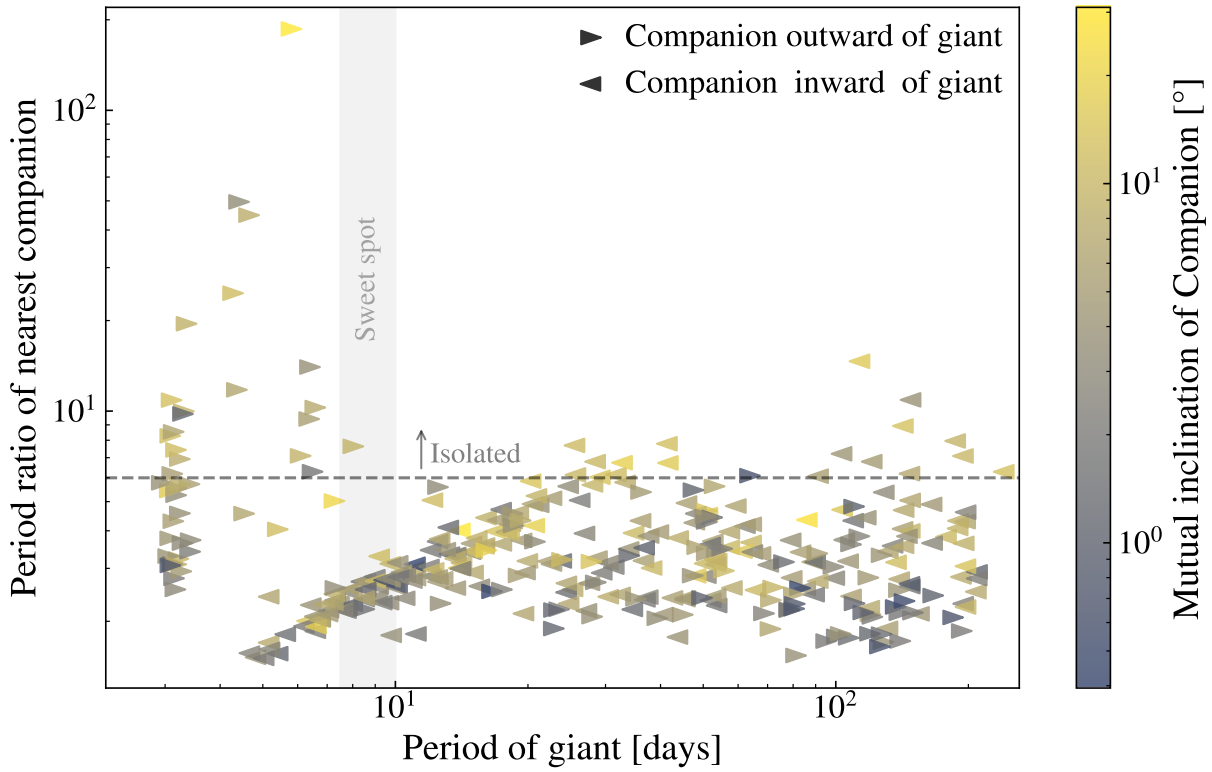

Figure 2. Final period ratios of our giants with their nearest companion as a function of final giant period. Right-pointed triangles indicate the nearest companion orbits exterior to the giant, while left-pointing triangles correspond to interior companions. The colors of the triangles correspond to the companions' orbital mutual inclinations (relative to the giant), and the horizontal dashed line indicates the isolation period ratio cut ($P_{j+1}/P_j = 6$) adopted in this work.

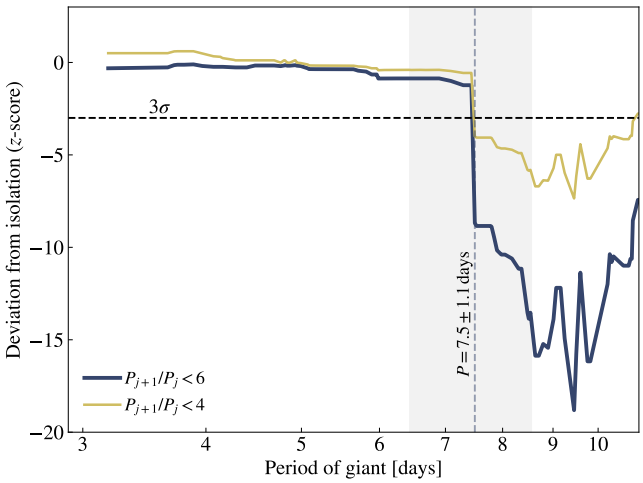

Figure 3. The statistical deviation from isolation for each sample of giants considered in our sliding bin test, as defined by the z-score of their period ratios relative to an isolation threshold of 6 (blue solid curve) and 4 (yellow dotted curve). The boundary beyond which giants are no longer statistically isolated ($\geqslant 3\sigma$ deviation, shown as the horizontal dashed line) is 7.5 ± 1.1 days (vertical dashed line) for the $P_{j+1}/P_j = 6$ threshold.

panionship dichotomy in our simulations. Considering a boundary driven by our simulation data also reduces the sensitivity of our results on our initial conditions — especially the period of the innermost planet, which is highly uncertain. For example, a modest shift of 1–2 days in our innermost periods may introduce a significant difference in the companionship statistics we computed in Section 3.1, despite introducing no meaningful difference in the evolution and final architectures of these systems.

3.3.1. *A Sweet Spot to Host Inner Companions*

In contrast with the isolated nature of hot Jupiters at $P < 7.5 \pm 1.1$ days, there is a dramatic ($\approx 8\sigma$) drop in the z-scores at periods just wide of this boundary, indicating a sharp transition to remarkably compact configurations for our giants. Indeed, the trough that follows (reaching $\approx 19\sigma$) represents the global minimum of our z-score testing, meaning that the population of giants orbiting just wide of the isolation boundary is the *least* isolated in our simulations. We find that these compact architectures are maintained at high significance ($> 5\sigma$) out to $P \approx 10$ days, manifesting as a tight cluster around period ratios of ≈ 2.5 in Figure 2. Notably, the nearest companions in this region ($P = 7.5$–10 days) tend

to reside on orbits interior to their giant counterpart (87.0%) and maintain low mutual inclinations (median $\mathcal{I}_{\rm mut} = 3.0°$), indicating this is a sweet spot to host transiting nearby inner companions.

Interestingly, we find that observed systems show good qualitative agreement with this sweet spot. As of this writing, all nine hot Jupiters known to reside in compact configurations with small planets host their nearby companion on an interior orbit, and only in one such system, WASP-47, has the presence of a small, nearby outer companion been confirmed. Furthermore, these giants with inner companions tend to occupy the long tail of the orbital period distribution for conventional hot Jupiters (Santerne et al. 2016; Yee & Winn 2023). Their minimum and mean periods of ≈ 4 days and ≈ 7 days, respectively, closely match our simulations, mimicking the transition beginning around $P \gtrsim 5$ days towards the highly compact architectures that dominate our companion 'sweet spot' at 7.5 days (see Figure 2).

3.4. *An Observational Dichotomy*

The nearby companion rates reported by previous hot and warm Jupiter demographics studies each consider companions in different orbital regimes: for transiting surveys, Huang et al. (2016) restricted their analysis to $P < 50$ days and Hord et al. (2021) considered both $P \leqslant 14$ days and $P < 50$ days, while the TTV study of Wu et al. (2023) adopted the period ratio range of $1.5 < P_{j+1}/P_j < 4$. As tabulated in Table 2, our multiplicity rates for nearby companions in these regimes also indicate a strong companionship dichotomy: compared to hot Jupiters, warm Jupiters host 1.4× more companions with $P < 50$ days, 2.1× more companions with $P \leqslant 14$ days, and 1.2× more companions with $P_{j+1}/P_j < 4$. Adopting our alternate hot Jupiter boundary of $P = 7.5$ days (see Section 3.3), these gaps widen to 1.5×, 2.5×, and 1.5×, respectfully.

Despite this general agreement with observations, we note that our multiplicity rates for both giant populations are significantly larger than observational expectations — especially for hot Jupiters. While Wu et al. (2023) place only a 12% lower limit on their nearby companion rate, this floor sits far below our estimates, as do the rates from Huang et al. (2016) and Hord et al. (2021) ($\sim$ 1–10%). However, the former study did not characterize their detection efficiency beyond $P_j/P_{j+1} \geqslant 4$ (where many of our companions reside; see Figure 2), and the latter two studies considered only coplanar companions with lower mutual inclinations (dispersions $\leqslant 2°$) than those found in this study (72% are $\geqslant 2°$). Therefore, we now investigate the detectability of our companions through transit, TTV, and, for completeness, radial velocity (RV) techniques. Rather than attempt population synthesis and rigorously apply our simulated results to a specific survey's completeness or detection pipeline (e.g., *Kepler*), we instead characterize how these three detection methods would modulate our observed companionship dichotomy.

Table 2. Simulated Nearby Companion Rates for Fiducial Simulations

Companion Regime	Hot Jupiters	Warm Jupiters
Conventional boundary ($P = 10$ days)		
True Rates		
$P \leqslant 14$ days	0.71±0.05	1.56±0.04
$P < 50$ days	1.52±0.09	2.17±0.06
$P_{j+1}/P_j < 4$	0.88±0.08	1.02±0.05
Co-transiting Rates		
$P \leqslant 14$ days	0.55±0.05	1.04±0.05
$P < 50$ days	0.70±0.06	1.23±0.06
Max isolation ($P = 7.5$ days)		
True Rates		
$P \leqslant 14$ days	0.60±0.07	1.51±0.04
$P < 50$ days	1.43±0.11	2.13±0.06
$P_{j+1}/P_j < 4$	0.70±0.09	1.05±0.05
Co-transiting Rates		
$P \leqslant 14$ days	0.41±0.05	1.03±0.04
$P < 50$ days	0.55±0.06	1.21±0.06

We first consider the geometric transit probability of our giants' companions. To determine whether a companion will transit, we adopt a similar approach to the methodology employed in Appendix D of Wu et al. (2023). First, assuming a circular orbit, we randomly select a transiting orbital inclination for the giant planet over $\theta_{\rm giant} \in \mathcal{U}(90° - \arctan(R_*/a), 90° + \arctan(R_*/a))$. Then, for each companion, we compute the associated inclination of the planet $\theta_{\rm comp}$ given their mutual inclination $\mathcal{I}_{\rm mut}$ and apply the following criterion: $90° - \arctan(\frac{R_*}{a(1-e^2)}) < \theta_{\rm comp} < 90° + \arctan(\frac{R_*}{a(1-e^2)})$, which takes into account the often non-negligible eccentricities of these small planets (Burke 2008). We repeat this process 10,000 times to get a robust transit probability $f_{\rm T}$ for each companion.

We plot the CDF of all probabilities for hot Jupiters and warm Jupiters in Figure 4. It is clear that the two distributions are discrepant, with a much larger fraction of warm Jupiters' companions having 100% transit likelihood. Following our methodology outlined in

Table 3. Summary of Companion Detectability Results for Fiducial Simulations

Metric	Hot Jupiters	Warm Jupiters	p
Conventional boundary ($P = 10$ days)			
All companions			
Median f_T (%)	22.1 ± 2.3	36.9 ± 1.6	10^{-4}
Median $K_{\rm RV}$ (m/s)	$2.55^{+0.14}_{-0.11}$	$3.33^{+0.12}_{-0.09}$	10^{-4}
Median $V_{\rm TTV}$ (min)	$2.53^{+2.37}_{-0.26}$	$11.31^{+10.37}_{-0.67}$	10^{-4}
Max isolation ($P = 7.5$ days)			
All companions			
Median f_T (%)	18.7 ± 2.6	36.2 ± 1.5	10^{-4}
Median $K_{\rm RV}$ (m/s)	$2.57^{+0.14}_{-0.13}$	$3.23^{+0.11}_{-0.08}$	10^{-4}
Median $V_{\rm TTV}$ (min)	$0.13^{+2.64}_{-0.01}$	$12.07^{+9.23}_{-0.68}$	10^{-4}

Section 3.1, we perform an AD test on the $f_{\rm T}$ distributions for these two giant populations. In Table 3, we report the median $f_{\rm T}$ values, as well as the p-value from our AD test, which together demonstrate that the companions of hot Jupiters are significantly less likely to be co-transiting (median $f_{\rm T} = 22.1 \pm 2.3\%$) compared to those of warm Jupiters (median $f_{\rm T} = 36.9 \pm 1.6\%$). This discrepancy increases when assuming our derived $P < 7.5$ days boundary for hot Jupiters instead of the conventional period (median $f_{\rm T} = 18.7 \pm 2.6\%$). Taking these probabilities into account, we recompute our multiplicity rates for co-transiting companions at $P \leqslant 14$ days and $P < 50$ days and include these values also in Table 2. Overall, we find closer agreement in both companion regimes due to a substantial fraction of companions that are not co-transiting ($\approx$ 30–60%), and fair ($\approx 2\sigma$) agreement between the $P \leqslant 14$ days hot Jupiter companion rate from Hord et al. (2021) ($7.3^{+15.2}_{-7.3}\%$) and our $P < 7.5$ days hot Jupiter rate ($40.5 \pm 5.4\%$). However, we note that the rest of our co-transiting rates remain significantly inflated relative to observations (at the $> 3\sigma$ level).

Next, we consider the TTVs of our giants, integrating each system for an additional 500 orbits with `rebound` and explicitly computing the "observed" transit timings of our giant planets (with a precision of $\leqslant 10$ seconds), assuming the observer is placed in the positive x-direction. We then take the difference between these observed values and their expected Keplerian values and calculate their root-mean-square to obtain the TTV amplitude $V_{\rm TTV}$. The middle panel of Figure 4 features the resulting CDFs for hot and warm Jupiters, which our AD test shows are also statistically distinct ($p \leqslant 10^{-4}$). We report the median $V_{\rm TTV}$ values in Table 3, which demonstrates that our warm Jupiters exhibit substantially larger TTVs compared to hot Jupiters, particularly those at $P < 7.5$ days. We find this discrepancy is most extreme for warm Jupiters at wider separations ($P \gtrsim 30$ days), where their typical amplitudes are enhanced by a factor of $100 - 1000\times$ compared to hot Jupiters'. This is consistent with the results of Wu et al. (2023), who demonstrated that the TTV signal-to-noise ratio increases with a planet's orbital period, although it is unclear whether this bias is capable of bringing our high $P_j/P_{j+1} < 4$ companion rates into agreement with theirs.

Finally, we also calculate analytically the RV semi-amplitude $K_{\rm RV}$, i.e., reflex motion, induced by each planet on the star, and plot their CDFs for hot Jupiters and warm Jupiters in Figure 4. Again, we find that these distributions are unique ($p \leqslant 10^{-4}$) and that the companions of warm Jupiters produce larger signals than those of hot Jupiters, though this discrepancy is modest compared to their relative transit fractions and TTV amplitudes (see median values in Table 3).

To summarize this section, we find that the transit, TTV, and RV methods all favor the detection of companions to warm Jupiters over hot Jupiters in our simulations, and hence may be expected to enhance the observed companionship dichotomy. This bias appears to be strongest for TTVs and transits, though we note that our analysis was limited in scope, as we consider only the geometric probability for transits, and the signal amplitudes of TTVs and RVs. In practice, the detectability of these companions depends also on the observational baseline, as it requires at least one ∼full orbit (i.e., for RVs) and often several orbits to yield a robust detection. Additionally, for each of these methods, the ability to extract the signal from an unknown small companion relies on accurate and precise knowledge of the giant's orbital and physical parameters, which is more easily obtained for closer-in giants. These biases may affect the relative nearby companion rates for hot and warm Jupiters in complex ways.

4. ADDITIONAL SIMULATIONS

4.1. *Varying the Initial Spacing*

Since the primordial compactness of our simulated systems, set by our adopted K value, is expected to play a significant role in shaping the systems' evolution, we ran two additional suites of 360-system simulations with slightly modified fiducial planet spacings: a more compact suite with $K = 8$ (see e.g., Kokubo & Ida 1995, 1998; Kokubo & Ida 2000) and a less compact suite with

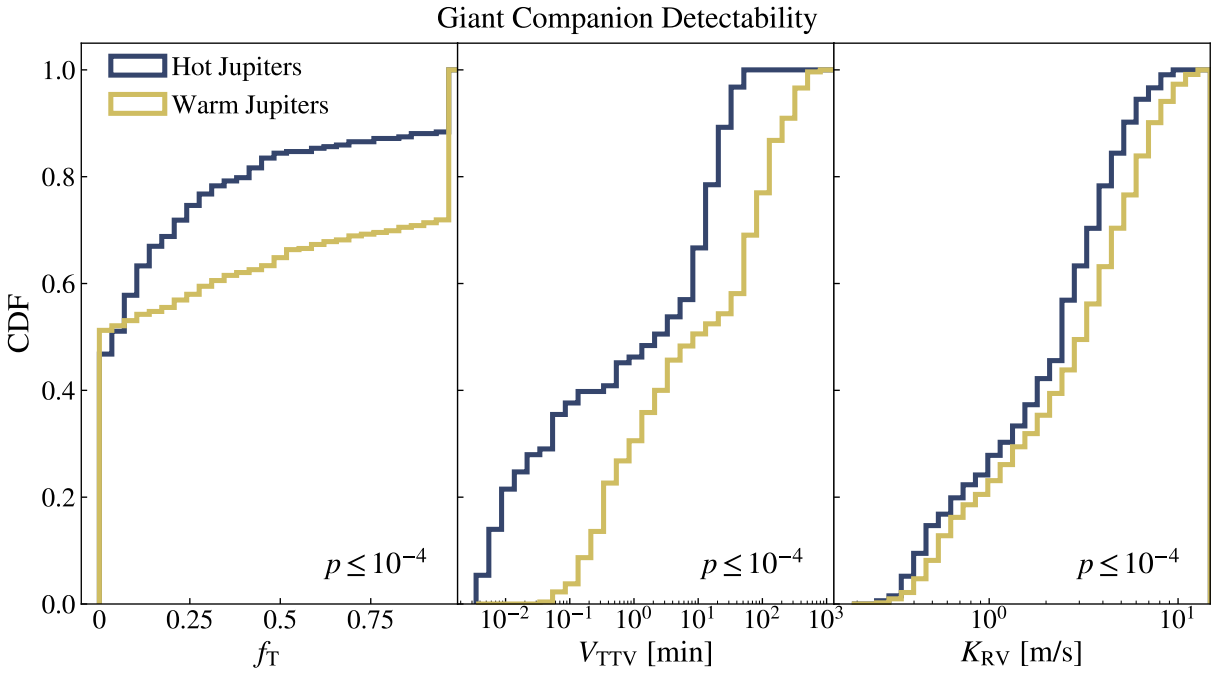

Figure 4. CDFs for the transit probabilities (left), TTV amplitudes (middle), and RV amplitude (right) of all remaining companions to hot Jupiters (blue) and warm Jupiters (yellow). In each panel, the p-values computed from our AD tests on the hot and warm Jupiter distributions are displayed in the bottom right.

$K = 12$. All other initial conditions were kept the same as our fiducial suite, described in Section 2. We present the main results of these non-fiducial simulations in Appendix 9. Ultimately, we find that changes to the initial planet spacing had little effect on our findings: the period ratio and mutual inclination distributions for hot Jupiter and warm Jupiter companions remain statistically distinct ($p \leqslant 0.005$), both skewing towards higher values for hot Jupiters.

4.2. *Tidal Forces*

To isolate the role of dynamical interactions in isolating hot Jupiters, we have excluded additional forces in our fiducial simulations. However, we note that tidal forces raised on the planets by the central star may play a significant role in sculpting the final architectures of our systems, potentially rapidly de-coupling highly eccentric small planets from their systems during phases of instability (Marzari & Nagasawa 2019) to create ultra-short-period planets (USPs; $P < 1$ days; Goyal & Wang 2025), or driving long-term, $\sim$ Gyr $-$ scale inward migration for our innermost ($P \lesssim 3$ days) hot Jupiters (e.g., Rasio et al. 1996; Levrard et al. 2009) or even their small companions (Pu & Lai 2019).

To investigate this effect, we include tidal forces using the `tides_constant_time_lag` model (Baronett et al. 2022) implemented in `reboundx` (Tamayo et al. 2020) with otherwise identical initial conditions to our $K = 10$ fiducial suite. We adopt Love numbers k_2 of 0.55 and 0.15 for our giants and small planets, respectively (see Becker & Batygin 2013). The constant time lag parameter, which is updated regularly for each planet throughout the simulation, is calculated as $\tau = 1/2nQ$ (Lu et al. 2023), where n is the orbital frequency and Q is the tidal quality factor, set to 10^5 for our giants and 10^4 for their companions (Millholland & Laughlin 2019).

We summarize the key companionship statistics for our simulations implementing this tidal effect in Appendix 9. Briefly, the inclusion of tidal forces leads to a modest increase in the strength of the hot Jupiter-warm Jupiter companionship dichotomy. Additionally, we find that a substantial fraction (17%) of our final companion population are USPs, including those interior to our 'sweet spot' hot Jupiters. Such a result is consistent with the emergence of several low-mass USPs (or near-USPs) with an outer hot Jupiter (e.g., WASP-47 c; Hellier et al. 2012 & Becker et al. 2015, WASP-132 c; Hellier et al. 2017 & Hord et al. 2022) or warm Jupiter (e.g., GJ-876 d; Laughlin et al. 2005, Rivera et al. 2010 & Millholland et al. 2018, Kepler-9 d; Holman et al. 2010 & Torres et al. 2011, 55 Cancri e; Marcy et al. 2002, Fischer et al. 2008 & Bourrier et al. 2018).

5. DYNAMICS

Each of our 12-planet systems experiences a dynamical instability that ultimately destroys one or more super-Earth companions. To characterize their dynamical histories, we track all multiplicity-changing events in our fiducial simulations. We identify four unique outcomes, each involving our small-planet companions: 1) collision with the host star (0.1%), 2) collision with the giant (12.4%), 3) collision with another companion (68.0%), or 4) ejection from the system (19.5%). While collisions generally dominate the inner regions and ejections become increasingly common in the outer regions (e.g., Gautham Bhaskar & Perets 2025) due to the planets' large Safronov numbers (Safronov 1972), we find that the position of the giant planet also bears strong influence over these outcomes. We therefore describe our systems' dynamical histories across three regimes based on the giant's initial position j in the system: hot Jupiters (j = 1–4), outer warm Jupiters (j = 9–12), and central warm Jupiters (j = 5–8).

We first consider the case of our hot Jupiters positioned at j = 1–4, which host long consecutive chains of 8–11 exterior small-planet companions. The giant quickly excites the eccentricity of its immediate neighbors to large values $\gg e_c$ (where e_c is the orbit crossing eccentricity of the system, see Equation 3). Due to its comparatively large mass, the giant's eccentricity remains near zero, these neighbors need to reach $e \approx 2e_c$ to collide with it, but only $e \approx e_c$ to collide with the next-closest small planet, provided that planet also reaches $e \approx e_c$. Since eccentricity is efficiently communicated between adjacent companions in their initial compact configurations ($K = 10$), the latter is favored, constituting 53% of outcomes for these nearest neighbors while the former constitutes 25% (and 0.3% collide with the star). At later times ($t \gtrsim 10^5 P_{\rm giant}$), a smaller, but non-negligible fraction (11%) are ejected from the system altogether (achieving $e > 1$), despite their close-in orbits.

Since $P_{\rm giant}$ is small relative to the orbital periods of companions comprising the exterior chain, the hot Jupiter's orbit alone effectively sets the dynamical timescale of the system, and the shorter this timescale is, the greater the eccentricity boost factor from dynamical stirring on faraway planets will be (see Equation 82 of Pu & Lai 2021). Consequently, large eccentricities ($e \gg e_c$) achieved by the giant's nearest exterior neighbor propagate outwards to progressively longer-period companions, triggering an instability cascade (beginning around $t \sim 10^4 P_{\rm giant}$) that is able to reach even the outermost companions. As seen in Figure 5, the outcomes of such global instability are diverse and only weakly dependent on orbital period: we find that even companions initially very distant from their hot Jupiter (e.g., $P \gtrsim 100$ days) can collide with it, and those initially on very close-in orbits ($P \lesssim 10$ days) can be ejected. Although the eccentricities of post-merger planets are damped by the collisional process (Matsumoto & Kokubo 2017), soon-to-be ejected planets on their journey out of the system, and the presence of many other nearby planets along the chain, help to induce further excitation and instabilities (beyond $t \gtrsim 10^7 P_{\rm giant}$). This results in a relatively flat final period ratio distribution that spans a large dynamic range. Additionally, the large eccentricities achieved by these companions are more readily 'converted' into inclinations (if $\gtrsim 3e_H$, where $e_H = r_H/a$ is the Hill's eccentricity), as demonstrated in Ida & Makino (1992), where an analogous set-up featuring a proto-planet swarmed by a field of co-planar planetesimals was adopted. This coupling between eccentricity and mutual inclination, shown in Figure 6, results in a large dispersion for the final mutual inclination distribution of hot Jupiters' companions.

In contrast, warm Jupiters, while still a dominant dynamical influence in their systems, have orbital periods that are larger compared to their companions. Therefore, $P_{\rm giant}$ represents a less important dynamical timescale, which now competes with the timescale set by the period of the innermost planet $P_{\rm inner}$ (Funk et al. 2010). Similarly to the case of hot Jupiters, most of the nearest neighbors are destroyed and $\approx 25\%$ collide with the giant, though a larger fraction now undergo ejection (23%) at later times rather than rapid collision with another companion (36%) due to the increased relative efficiency of ejections at longer periods (Li et al. 2020; Pu & Lai 2021). The longer orbital periods of warm Jupiters diminish their ability to propagate their eccentricity inward, so in the regime where $P_{\rm inner} \ll P_{\rm giant}$ (i.e., outer warm Jupiters at j = 9–12), the innermost companion dominates the evolution of the inner system. With minimal influence from the outer giant, it is difficult for these planets to achieve $e \gg e_c$, so companion-companion collisions dominate the inner regions (within $P < 30$ days) while ejections and giant collisions are limited to the outer regions. Therefore, the global instability phase is shorter (ending by $t \sim 10^7 P_{\rm giant}$) and less chaotic compared to that of hot Jupiters, and post-merger eccentricities more often stay damped, resulting in final period ratio and mutual inclination distributions that are peaked toward lower values with less dispersion.

Closer-in, central warm Jupiters (j = 5–8) initially host an inner and outer chain of 4–5 planets which are effectively dynamically isolated since the nearly-circular giant suppresses eccentricity communication across its orbit. Although these giants carry greater influence over

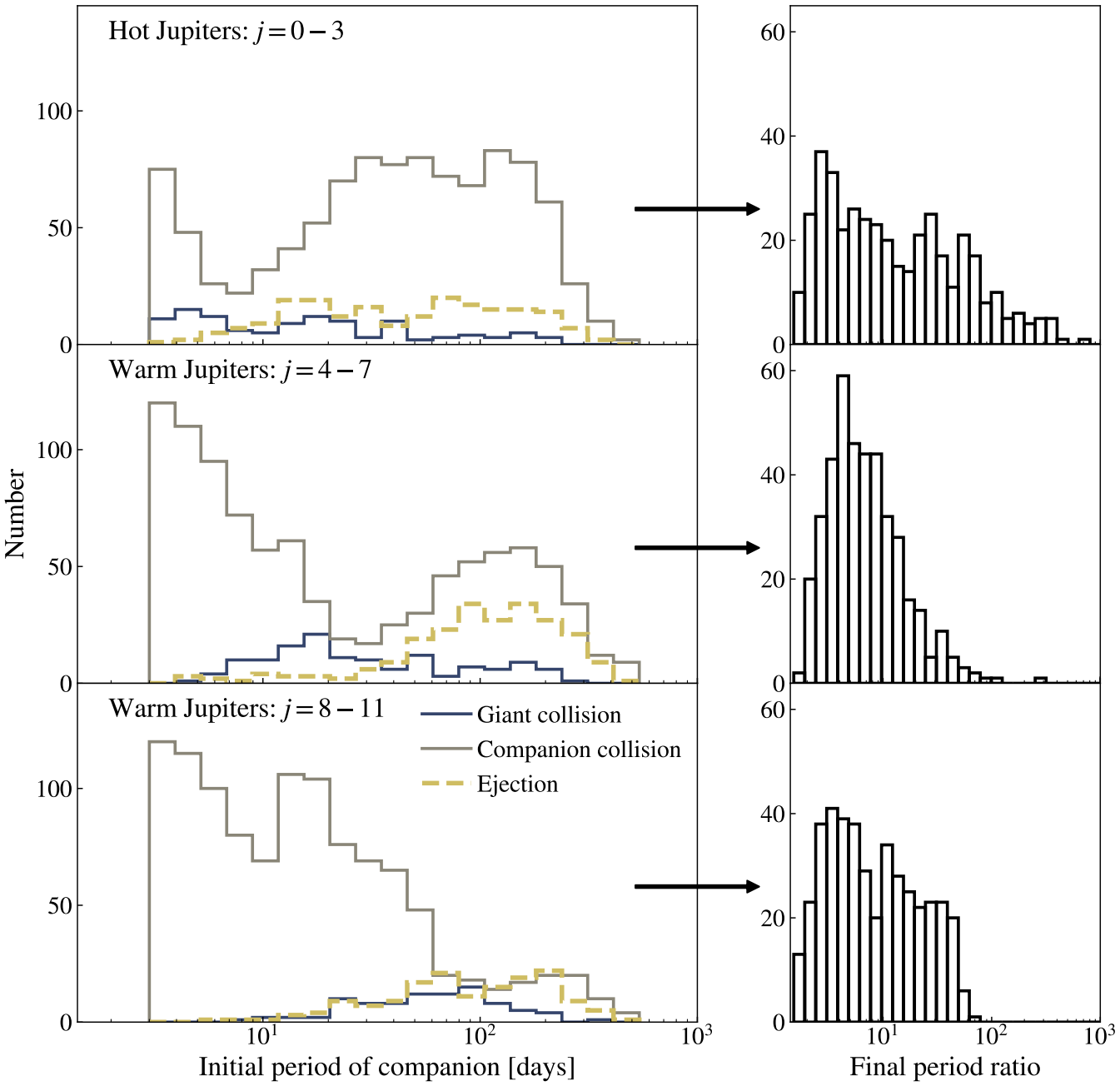

Figure 5. Instability outcomes as a function of initial orbital period (left column) and final period ratio distributions (right column) for our companions, plotted separately for hot Jupiters (positioned at j = 1–4; top row), central warm Jupiters (at j = 5–8; middle row), and the outermost warm Jupiters (at j = 9–12; bottom row). In the left-hand column panels, companion-giant collisions (blue solid line), companion-companion collisions (grey solid line), and companion ejections (yellow dashed line) are displayed (companion-star collisions are negligible). It is apparent that instability outcomes vary according to the location of the giant planet in our multi-super-Earth systems. Globally, the companions of hot Jupiters experience the widest variety of instability outcomes (driven by nominal propagation of high eccentricities along the exterior planet chain), causing their final period ratio and mutual inclination distributions to exhibit larger dispersions.

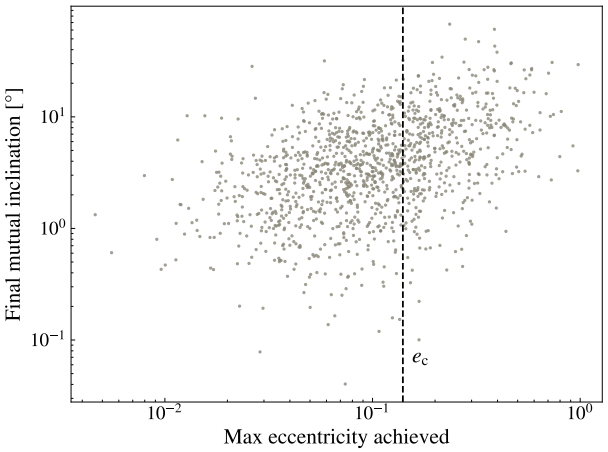

Figure 6. The mutual inclinations of each surviving giant companion at the end of the simulation as a function of the maximum eccentricity reached by that companion (after any mergers), with the orbit-crossing eccentricity plotted as a dashed vertical line. The strong visible correlation demonstrates that larger eccentricities, which are more often achieved by hot Jupiters' companions, lead to inflated mutual inclinations.

the evolution of the inner system compared to the outermost warm Jupiters, $P_{\rm inner}$ is still important and there are fewer overall interacting bodies within the chain, so companion-companion collisions are generally favored and post-merger objects have a higher tendency to be stable. The evolution of the exterior chain is analogous to that of the hot Jupiter chain, though scaled down and with a higher ejection frequency. The net result is a final period ratio distribution that is more highly-peaked and with a lower overall median value than that of both hot Jupiters and the outermost warm Jupiters (note this partially reflects their initial period ratio distributions; see Section 6.1.1 below), and a mutual inclination distribution that is intermediate to that of hot Jupiters and the outermost warm Jupiters.

In summary, we find that the combination of hot Jupiters' short dynamical timescale ($P_{\rm giant}$) and long outer companion chain optimizes the global communication and re-excitation of large eccentricities ($e \gg e_{\rm c}$), which can explain their companions' enhanced period ratios and mutual inclinations relative to warm Jupiters.

5.1. *Creation of a Sweet Spot for Hot Jupiters*

The giant's ability to suppress eccentricity communication can also explain the propensity for hot Jupiters at $P = 7.5$–10 days to end up with nearby, co-transiting inner companions. Due to their initial positions ($j = 3$–4), these giants begin post-disk evolution with either two or three interior companions. These short companion chains will undergo dynamical instabilities, quickly reducing themselves to one planet largely through some combination of collisions (see top panel of Figure 5). Since the giant dynamically isolates planets on opposing sides of it, there is no mechanism to excite the eccentricity (or mutual inclination) of the remaining inner companion, and it will effectively become part of a two-body system with the giant. The resulting spacing is of order $K' \sim 2K \gg 2\sqrt{3}$, so the pair will be Hill stable indefinitely and the hot Jupiter will retain this nearby inner companion throughout its system's evolution. As is visible in Figure 2, there is no analogous sweet spot for warm Jupiters (at $j = 9$–10); this is because a large fraction of their outer companions instead undergo ejection from the system during the instability phase (see bottom panel of Figure 5).

5.2. *Tides Destroy or Detach Highly Eccentric Planets*

The inclusion of planetary tides has a small, but measurable effect on our systems' dynamical evolution. Since the tidal gravitational force experienced by a planet scales sensitively with heliocentric distance, high-eccentricity planets ($e \gg e_{\rm c}$) with small periastron can rapidly dissipate orbital energy and decouple from the rest of the system. Our hot Jupiters are more effective in exciting large eccentricities along their super-Earth chains, so tides play a more significant role in the evolution of their companions. Exterior planets experiencing such orbital decay are more likely to collide with or be ejected by the giant, while planets on the interior become detached from the hot Jupiter to become USPs. In addition, some hot Jupiters experience small inward motion due to tidally-induced orbital decay. As a result, both the period ratio and mutual inclination distributions for hot Jupiter companions end up inflated relative to the fiducial results (as discussed in Section 4.2), creating an exaggerated companionship dichotomy.

6. DISCUSSION

6.1. *Caveats*

6.1.1. *The Mirror Effect*

Due to the EMS scheme adopted in this work (see Section 2), the initial companion period ratios for giants occupying the nth innermost position in their 12-planet system (at position j) mirrors those of giants in the nth outermost position (at position $13 - j$). Consequently, giants placed near the edges of their systems begin with period ratio distributions that exhibit more variance and a higher overall median than those embedded near the centers, whose distributions are comparatively concentrated at lower values. Therefore, any cut that breaks this symmetry will result in samples with disparate initial period ratio distributions. In this way,

our hot Jupiters (at $P < 10$ days), which initially occupy only the innermost four positions ($j = 1$–4) in their systems, are predisposed to end up with more sparsely spaced companions than warm Jupiters, which jointly contain giants positioned in both the outermost four spots ($j = 9$–12) as well as the central four spots ($j = 5$–8) of their systems.

To characterize the influence of this mirror effect on our results, we plot in Figure 7 the median companion period ratios of our inner giants (ordered from $j = 1$–6) against those of our outer giants (ordered from $j = 12$–7), along with a 1:1 line for comparison. Indeed, we find there is an apparent correlation between these median values, and that there is strong symmetry for giants initially near the center of their systems. However, it is clear that those closer to the edge show increasingly significant deviation from the 1:1 expectation. Critically, we see that, even controlling for our giants' natal proximity to the edge of their multi-planet system, hot Jupiters' period ratios consistently skew to higher values than warm Jupiters', exhibiting both larger medians and upper errors. This is also apparent when comparing the final period ratio distributions of our $j = 1$–4 giants against our $j = 9$–12 giants in Figure 5. Therefore, the preferential isolation of hot Jupiters is largely dynamics-driven (see Section 5).

Although the initial mutual inclination distribution is independent of the giant's position, the final distribution is determined by the dynamical evolution process, which depends on how deeply embedded the giant is in its multi-planet system (as discussed in Section 5). Figure 7 also features a comparison of the median mutual inclinations for our inner and outer giants, which again shows a rightward skew relative to the 1:1 line, demonstrating the role of dynamical evolution in producing the enhanced inclinations of companions to hot Jupiters.

6.1.2. *Final Stability*

To achieve comparable dynamical ages, each system was integrated to $10^9 P_{\rm giant}$. However, as discussed in Section 5, $P_{\rm inner}$ represents an important dynamical timescale as well, especially in the limit $P_{\rm inner} \ll P_{\rm giant}$. The net effect is that our systems with longer-period giants tend to be more dynamically mature than those with closer-in giants. To characterize this effect, we use the SPOCK machine-learning tool (Stability of Planetary Orbital Configurations Classifier; Tamayo et al. 2020) to predict the orbital stability of our final systems. We calculate an instability fraction of 25% for our hot Jupiter systems and 18% for our warm Jupiter systems, indicating that we may have underestimated the preferential isolation of our hot Jupiters, which are more likely to experience further instabilities.

6.2. *Origins*

Such an interpretation is also independently supported by measurements of stellar obliquity, which demonstrate that some hot Jupiters are significantly spin-orbit misaligned (Winn et al. 2010; Rice et al. 2022) while warm Jupiters appear to ubiquitously be in alignment (Rice et al. 2022; Wang et al. 2024).

Recent observations, however, have revealed an increasing number of hot Jupiters with nearby companions (e.g., WASP-47 b; Becker et al. 2015, Kepler-730 b; Cañas et al. 2019, TOI-1130 c; Huang et al. 2020, WASP-148 b; Hébrard et al. 2020, TOI-2494 c, TOI-5143 c; Guerrero et al. 2021, Quinn et al in prep., WASP-132 b; Hord et al. 2022, TOI-2000 c; Sha et al. 2023, WASP-84 b; Maciejewski et al. 2023, TOI-1408 b; Korth et al. 2024), and the latest search for transit timing variations in the full *Kepler* data set found that at least $12 \pm 6\%$ of hot Jupiters host nearby companions (Wu et al. 2023). Such findings, coupled with the emerging trend of strict spin-orbit alignment for hot Jupiters in compact configurations (Sanchis-Ojeda et al. 2015; Anderson et al. 2015; Radzom et al. 2025), suggest that a substantial fraction of these close-in giants may also have quiescent histories.

The mechanism by which giants can emerge from the disk embedded in such high-multiplicity, compact systems as adopted in this work is unclear. Considering first the in situ formation scenario, it has been demonstrated that the critical mass required for a rocky core to undergo runaway gas accretion (Pollack et al. 1996) is only weakly dependent on nebular conditions (Stevenson 1982; Rafikov 2006), meaning that giant planet formation may be viable across a broad range of orbital separations (Lee et al. 2014).

Since the runaway accretion process is expected to be relatively rapid, even close in to the star ($< 10^5$ yr; e.g., Lee & Chiang 2015; Batygin et al. 2016), in-situ formation for giants hinges largely on whether a critical-mass core (e.g., ~ 10–$30\,M_\oplus$) can be formed before the disk dissipates. The solid accretion timescale of the core and the disk removal timescale depend on many uncertain variables, including the disk's structure and composition. Provided there is a sufficient reservoir of solid material in the innermost regions of the disk (see Chiang & Laughlin 2013; Schlichting 2014), there are several promising mechanisms to assemble massive super-Earth cores on timescales $\lesssim 1$ Myr (Lambrechts & Johansen 2012, 2014; Lenz et al. 2019; Zawadzki et al. 2021) — i.e., well within the typical disk lifetime of 1–10 Myr (Haisch

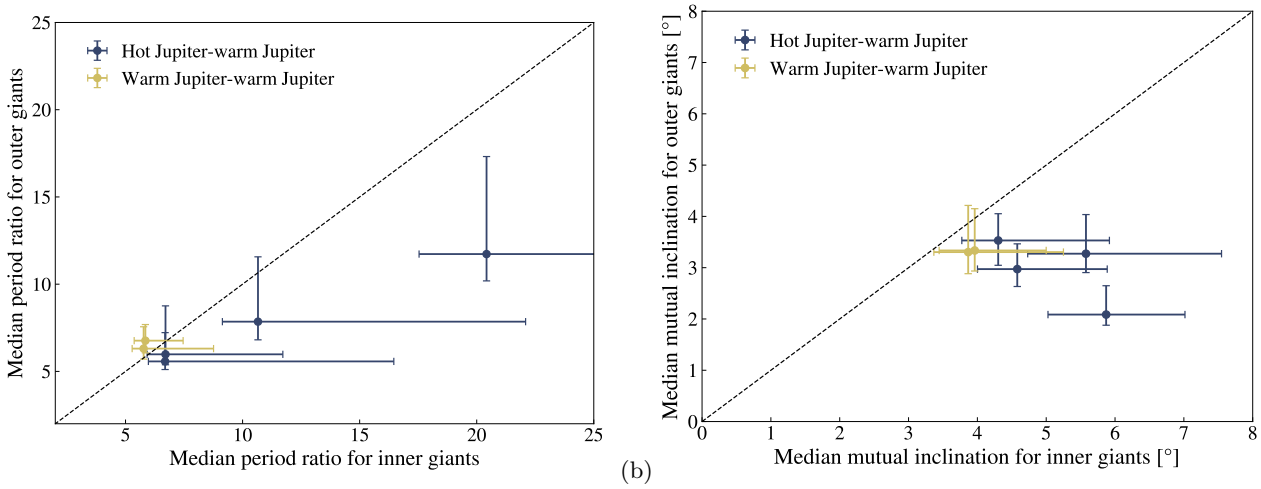

Figure 7. (a) Median period ratio comparison and (b) median mutual inclination comparison for giants positioned in the innermost six spots against the outermost six spots, with standard errors and 1:1 lines included (dashed black line). Blue points represent comparisons across the $P = 10$ days hot Jupiter-warm Jupiter boundary, while yellow points correspond to comparisons between warm Jupiters only. The significant rightward deviation of the blue points from the 1:1 line demonstrates that hot Jupiters generate both higher period ratios and mutual inclinations for their companions compared to warm Jupiters, even when controlling for their initial proximity to their systems' edges (i.e., how deeply embedded in their systems they are).

et al. 2001; Jayawardhana et al. 2006; Currie et al. 2009). This is especially true for more massive disks, which not only likely have more solid mass but also generally have longer lifetimes (Bayo et al. 2012; Ribas et al. 2015; Ben et al. 2025), potentially lowering the critical core mass needed for runaway accretion (Lee & Chiang 2015).

Regardless, the tight orbital configurations of our giant planets within their multi-planet systems may trigger an instability that halts the runaway accretion process, preventing such an architecture from being realized. While the random enhancements we introduce to the mutual Hill spacing of our giant planets ($\delta K \sim K$) helps to account for this, we find that the time for one or more companions to reach $e = e_c/2$, which we take as the dynamical instability growth time $t_{\rm dyn}$, is $\sim$ 10–100 yr. Although this is short compared to the runaway accretion timescale $t_{\rm acc} \sim 10^4$–10^5 yr (Batygin et al. 2016), gaseous disks have an eccentricity-damping effect that stabilizes planetary orbits (Ward 1997; Chatterjee et al. 2008), even in the presence of a giant (Li et al. 2024). For our super-Earths, the eccentricity-damping timescale $t_{\rm damp}$ is expected to be $\sim 10^2$yr (Goldberg & Batygin 2022), which is comparable to $t_{\rm dyn}$. In principle, since this damping efficiency decreases linearly with increasing planet mass (Matsumura et al. 2010), $t_{\rm damp}$ should be even shorter for our growing giants, ensuring stability throughout the runaway accretion phase. However, if the giant clears a gap in the disk, this damping effect too will vanish, allowing for rapid eccentricity excitation (Moorhead & Adams 2008; Matsumura et al. 2010), which may stunt the proto-giant's growth. In any case, if the giant is able to form in situ prior to the onset of instability, it seems inevitable that hot Jupiters become observationally isolated relative to warm Jupiters — either due to sweeping secular resonances in the limit of low multiplicity, as demonstrated in Batygin et al. (2016), or due to long-term post-disk dynamics, as shown in this work.

A possible contradiction of the in situ model is that rocky planets embedded in a gas-rich disk are subject to Type I orbital migration (Artymowicz 1993; Ward 1997; Terquem & Papaloizou 2007; Ida & Lin 2008; Ida & Lin 2010; McNeil & Nelson 2010), which can only be avoided in a gas-poor or dissipating disk (Raymond et al. 2008; Chiang & Laughlin 2013; Raymond & Cossou 2014), but such an environment lacks the necessary conditions for runaway accretion. Further, chains of multiple super-Earths are expected to undergo convergent migration and subsequently lock into first-order MMRs (e.g., 3:2 or 2:1; Lee & Peale 2002; Terquem & Papaloizou 2007; Raymond et al. 2008; McNeil & Nelson 2010), which are later broken by mutual interactions after the disk disappears (Kominami & Ida 2004; Iwasaki & Ohtsuki 2006; Izidoro et al. 2017; Izidoro et al. 2021). Due to our systems' high multiplicity and short instability timescale, the initial proximity of our super-Earths to MMR, and hence whether they initially migrated in resonant chains, will not have a significant effect on our result (see also Matsumoto et al. 2012). The presence of a migrating giant, however, may have important implications.

Disk-driven migration allows proto-hot and -warm Jupiters to form farther out in the disk, near the peak

of the observed giant occurrence rate ($\sim$ 2–3 AU; Fernandes et al. 2019; Fulton et al. 2021), where the conditions for core agglomeration are more favorable (Hayashi 1981; Pollack et al. 1996; Kokubo & Ida 2002; Masset et al. 2006), and the instability growth timescale is longer. Upon clearing a gap, continuous angular momentum exchange with the disk will bring the giant inward to short orbital periods on timescales of 10^5–10^6 yr, as described by the Type II migration paradigm (Goldreich & Tremaine 1979; Lin & Papaloizou 1986, 1993; Lin et al. 1996). While super-Earths born interior to the proto-giant will be able to freely migrate inwards (on timescales of $\sim 10^5$ yr; e.g., Goldberg & Batygin 2022), the giant acts to block inward-moving exterior companions, which will cause a pile-up of outer planets that is susceptible to strong mutual gravitational interactions (Izidoro et al. 2015). In addition to collisions and ejections, such instability may result in 'jumpers', i.e., outer super-Earths capable of crossing the giant's orbit to end up in the inner disk. This outcome is expected to be more common for outer systems with higher initial multiplicities (e.g., containing $\geqslant 5$ super-Earths; Izidoro et al. 2015). Therefore, while disk migration may cause preliminary clearing of outer companions, it may also transport some to interior orbits, increasing the initial length of the inner super-Earth chain and hence the likelihood for our giants to host inner companions. For the case of our outermost giants ($j \gtrsim 10$), which begin with few outer companions and long inner companion chains, disk migration should have relatively little effect on the initial architecture.

Nevertheless, the ability of this quiescent, compact model to explain the observed preferential isolation of hot Jupiters warrants further exploration. High-eccentricity migration models require interactions with a massive external perturber and, in the case of single-star systems, a distant outer giant planet (beyond several AU), which appear to be under-abundant in hot Jupiter systems (Ngo et al. 2016; Schlaufman & Winn 2016; however, see also Bryan et al. 2016). A generic observational prediction from this work is that quiescently-formed short-period giants should host a substantial population of hidden, non-transiting companions (see Section 3.4) — which we note may have larger mutual inclinations than predicted here due to stellar rotation-driven dynamics (MacLean & Becker 2025). Critically, many of these companions are close-in ($P \lesssim 50$ days), requiring a substantially shorter observational baseline for discovery compared to cold giants. While RVs and TTVs may both be capable of detecting such inclined companions, caution must be exercised, as both methods are significantly biased against hot Jupiters in our simulations. However, given that this discrepancy is smallest for RVs, future high-precision ($\sim$ 1 m/s) Doppler searches are likely the most effective means of unveiling such companions and, therefore, validating this model.

7. CONCLUSIONS

We have demonstrated that, through long-term dynamical evolution (10^9 orbits) in compact multi-planet systems, hot Jupiters will naturally self-isolate relative to warm Jupiters, generating both larger period ratios and mutual inclinations for their planetary companions. Altogether, compared to warm Jupiter companions, we find these planets will be more difficult to detect with modern methods. These phenomena can be summarized by the following key findings from our fiducial simulations:

1. The period ratio and mutual inclination distributions of companions to hot Jupiters and warm Jupiters in our simulations are statistically distinct ($p \leqslant 10^{-4}$), with $\approx 60\%$ higher median values for hot Jupiters.

2. Compared to those of warm Jupiters, the companions of hot Jupiters are also significantly ($p \leqslant 10^{-4}$) more difficult to detect via transits, radial velocities, and transit timing variations. For transits, this discrepancy is especially strong for close-in companions ($P < 50$ days), where the observed companion rates can differ by a factor of $\approx 2\times$.

These results show that a significant companionship dichotomy can be achieved without dichotomous origins for hot and warm Jupiters, and instead through a unified quiescent paradigm. Accordingly, preferential isolation for hot Jupiters is not unique to violent origins such as high-eccentricity migration. In addition, we found that quiescently-formed hot Jupiters embedded in compact, high-multiplicity systems can qualitatively reproduce the peculiar architectures of hot Jupiters known to host small, nearby companions, which are often on interior orbits (e.g., Kepler-730 b, TOI-1130 c, TOI-2494 c, TOI-5143 c, WASP-132 b, TOI-2000 c, WASP-84 b, and TOI-1408 b). Agreement with observed configurations, including giants with USP companions, is improved when the effect of planetary equilibrium tides is taken into account, which also enhances the companionship dichotomy.

Despite these successes, several challenges to this unified model remain. First, we find that it significantly over-predicts the co-transiting companion multiplicity rates for both hot and warm Jupiters (by as much as $\sim 10\times$). Further, there are several theoretical uncertainties regarding the conditions under which, assuming

either in situ formation or disk migration, a short-period gas giant can emerge from the disk with nearby super-Earth chains. However, we emphasize that the disparate dynamical evolution we found for hot and warm Jupiter systems — particularly the enhanced ability of shorter-period, inner giants to excite large eccentricities globally — should be robust to the precise initial formation conditions. Continued discoveries enabled by TESS, paired with high-precision RV follow-up campaigns, will help constrain the true companion rate of hot Jupiters and warm Jupiters and hence provide insight into their origins.

We would like to thank André Izidoro for his insightful discussion related to this work, as well as Armaan Goyal for his expertise regarding statistical methods.

This research has made use of the NASA Exoplanet Archive, which is operated by the California Institute of Technology, under contract with the National Aeronautics and Space Administration under the Exoplanet Exploration Program. M.R. and S.W. thank the Heising-Simons Foundation for their generous support. This research was supported in part by Lilly Endowment, Inc., through its support for the Indiana University Pervasive Technology Institute. D.W. is supported by the National Natural Science Foundation of China (NSFC) (grant No. 12103003).

8. APPENDIX A: ENERGY AND ANGULAR MOMENTUM CONSERVATION

`TRACE` is a hybrid integrator that utilizes the symplectic Wisdom-Holman integrator `WHFast` (Rein & Tamayo 2015) for secular interactions and switches to a higher-order scheme when the minimum mutual Hill separation between any two bodies falls below a certain threshold. To ensure we achieve the best-possible accuracy during phases of instability, we adopt a conservative switching threshold of $r_{H,\mathrm{mut}} < 7$, and switch to the 15th-order adaptive-step `IAS15` integrator (Rein & Spiegel 2015) rather than the adaptive-step (and adaptive-order) Gragg-Bulirsch-Stoer scheme (Press et al. 2003). We retain the default value of 10^{-9} for `IAS15`'s dimensionless precision parameter ϵ_b (Rein & Spiegel 2015), which corresponds to a nominal relative energy error after one timestep of 8.9×10^{-34} (see their Eq. 23), though in practice the minimum relative error has a floor of 10^{-16}. We note that this default value for ϵ_b is selected such that this machine precision is expected to be maintained even after $\sim 10^{10}$ dynamical times (orbits) and with multiple bodies having eccentric orbits (Rein & Spiegel 2015). We set the maximum timestep to $P_{\mathrm{giant}}/15$ (no minimum timestep is specified). For `WHFast`, we set the fixed timestep to 1/15th of the initial innermost period of our systems (consistent with recommendations from Rein & Tamayo 2015). For our fiducial suite, we compute median relative energy and angular momentum errors of 1.3×10^{-4} and 3.9×10^{-2}, respectively, but find that the latter is dominated by the removal of ejected planets. The maximum energy error achieved is 3.4×10^{-3}, indicating good accuracy overall.

Table 4. Summary of Key Companionship Results for Non-Fiducial Simulations

Metric[a]	Hot Jupiters	Warm Jupiters	p
$K = 8$			
All companions			
Median P_{j+1}/P_j	XX	XX	XX
Median $\mathcal{I}_{\mathrm{mut}}$ (°)	XX	XX	XX
Nearest companions			
Median P_{j+1}/P_j	XX	XX	XX
Median $\mathcal{I}_{\mathrm{mut}}$ (°)	XX	XX	XX
$K = 12$			
All companions			
Median P_{j+1}/P_j	XX	XX	XX
Median $\mathcal{I}_{\mathrm{mut}}$ (°)	XX	XX	XX
Nearest companions			
Median P_{j+1}/P_j	XX	XX	XX
Median $\mathcal{I}_{\mathrm{mut}}$ (°)	XX	XX	XX
$K = 10$ With Tides			
All companions			
Median P_{j+1}/P_j	XX	XX	XX
Median $\mathcal{I}_{\mathrm{mut}}$ (°)	XX	XX	XX
Nearest companions			
Median P_{j+1}/P_j	XX	XX	XX
Median $\mathcal{I}_{\mathrm{mut}}$ (°)	XX	XX	XX

[a] Note that, for simplicity, we only report our non-fiducial results adopting the conventional hot Jupiter-warm Jupiter boundary of $P = 10$ days.

9. APPENDIX B: NON-FIDUCIAL RESULTS

We compile all key companionship statistics for our non-fiducial simulations in Table 4.

REFERENCES

Anderson, D. R., Triaud, A. H. M. J., Turner, O. D., et al. 2015, ApJL, 800, L9, doi: 10.1088/2041-8205/800/1/L9

Artymowicz, P. 1993, ApJ, 419, 166, doi: 10.1086/173470

Bailey, E., & Batygin, K. 2018, ApJL, 866, L2, doi: 10.3847/2041-8213/aade90

Baronett, S. A., Ferich, N., Tamayo, D., & Steffen, J. H. 2022, MNRAS, 510, 6001, doi: 10.1093/mnras/stac043

Batygin, K., Bodenheimer, P. H., & Laughlin, G. P. 2016, ApJ, 829, 114, doi: 10.3847/0004-637X/829/2/114

Bayo, A., Barrado, D., Huélamo, N., et al. 2012, A&A, 547, A80, doi: 10.1051/0004-6361/201219374

Becker, J. C., & Batygin, K. 2013, The Astrophysical Journal, 778, 100, doi: 10.1088/0004-637X/778/2/100

Becker, J. C., Vanderburg, A., Adams, F. C., Rappaport, S. A., & Schwengeler, H. M. 2015, ApJL, 812, L18, doi: 10.1088/2041-8205/812/2/L18

Ben, G. M., Jose, J., & Hernández, J. 2025, MNRAS, 541, 2246, doi: 10.1093/mnras/staf1089

Boley, A. C., Contreras, A. P. G., & Gladman, B. 2016, The Astrophysical Journal, 817, L17, doi: 10.3847/2041-8205/817/2/l17

Bourrier, V., Dumusque, X., Dorn, C., et al. 2018, A&A, 619, A1, doi: 10.1051/0004-6361/201833154

Bryan, M. L., Knutson, H. A., Howard, A. W., et al. 2016, ApJ, 821, 89, doi: 10.3847/0004-637X/821/2/89

Burke, C. J. 2008, ApJ, 679, 1566, doi: 10.1086/587798

Cañas, C. I., Wang, S., Mahadevan, S., et al. 2019, ApJL, 870, L17, doi: 10.3847/2041-8213/aafa1e

Chambers, J., Wetherill, G., & Boss, A. 1996, Icarus, 119, 261, doi: https://doi.org/10.1006/icar.1996.0019

Chatterjee, S., Ford, E. B., Matsumura, S., & Rasio, F. A. 2008, ApJ, 686, 580, doi: 10.1086/590227

Chiang, E., & Laughlin, G. 2013, MNRAS, 431, 3444, doi: 10.1093/mnras/stt424

Currie, T., Lada, C. J., Plavchan, P., et al. 2009, ApJ, 698, 1, doi: 10.1088/0004-637X/698/1/1

Darling, D. A. 1957, The Annals of Mathematical Statistics, 28, 823 , doi: 10.1214/aoms/1177706788

Dawson, R. I., & Johnson, J. A. 2018, ARA&A, 56, 175, doi: 10.1146/annurev-astro-081817-051853

Egmann, S., & Cousineau, D. 2011, Journal of Applied Quantitative Methods, 6, 918. https://jaqm.ro/issues/volume-6,issue-3/1_engmann_cousineau.php

Fabrycky, D., & Tremaine, S. 2007, ApJ, 669, 1298, doi: 10.1086/521702

Feigelson, E. D., & Babu, G. J. 2013, in Planets, Stars and Stellar Systems. Volume 2: Astronomical Techniques, Software and Data, ed. T. D. Oswalt & H. E. Bond, 445, doi: 10.1007/978-94-007-5618-2_10

Fernandes, R. B., Mulders, G. D., Pascucci, I., Mordasini, C., & Emsenhuber, A. 2019, ApJ, 874, 81, doi: 10.3847/1538-4357/ab0300

Fischer, D. A., Marcy, G. W., Butler, R. P., et al. 2008, ApJ, 675, 790, doi: 10.1086/525512

Fulton, B. J., Rosenthal, L. J., Hirsch, L. A., et al. 2021, ApJS, 255, 14, doi: 10.3847/1538-4365/abfcc1

Funk, B., Wuchterl, G., Schwarz, R., Pilat-Lohinger, E., & Eggl, S. 2010, A&A, 516, A82, doi: 10.1051/0004-6361/200912698

Gautham Bhaskar, H., & Perets, H. 2025, arXiv e-prints, arXiv:2501.13166, doi: 10.48550/arXiv.2501.13166

Gladman, B. 1993, Icarus, 106, 247, doi: 10.1006/icar.1993.1169

Goldberg, M., & Batygin, K. 2022, The Astronomical Journal, 163, 201, doi: 10.3847/1538-3881/ac5961

Goldreich, P., & Tremaine, S. 1979, ApJ, 233, 857, doi: 10.1086/157448

Goyal, A. V., & Wang, S. 2025, The Astronomical Journal, 169, 191, doi: 10.3847/1538-3881/adb487

Guerrero, N. M., Seager, S., Huang, C. X., et al. 2021, ApJS, 254, 39, doi: 10.3847/1538-4365/abefe1

Haisch, Jr., K. E., Lada, E. A., & Lada, C. J. 2001, ApJL, 553, L153, doi: 10.1086/320685

Hamers, A. S., Antonini, F., Lithwick, Y., Perets, H. B., & Portegies Zwart, S. F. 2017, MNRAS, 464, 688, doi: 10.1093/mnras/stw2370

Hayashi, C. 1981, Progress of Theoretical Physics Supplement, 70, 35, doi: 10.1143/PTPS.70.35

Hébrard, G., Díaz, R. F., Correia, A. C. M., et al. 2020, A&A, 640, A32, doi: 10.1051/0004-6361/202038296

Hellier, C., Anderson, D. R., Collier Cameron, A., et al. 2012, MNRAS, 426, 739, doi: 10.1111/j.1365-2966.2012.21780.x

—. 2017, MNRAS, 465, 3693, doi: 10.1093/mnras/stw3005

Holman, M. J., Fabrycky, D. C., Ragozzine, D., et al. 2010, Science, 330, 51, doi: 10.1126/science.1195778

Hord, B. J., Colón, K. D., Kostov, V., et al. 2021, AJ, 162, 263, doi: 10.3847/1538-3881/ac2602

Hord, B. J., Colón, K. D., Berger, T. A., et al. 2022, AJ, 164, 13, doi: 10.3847/1538-3881/ac6f57

Hou, A., Parker, L. C., Harris, W. E., & Wilman, D. J. 2009, ApJ, 702, 1199, doi: 10.1088/0004-637X/702/2/1199

Huang, C., Wu, Y., & Triaud, A. H. M. J. 2016, ApJ, 825, 98, doi: 10.3847/0004-637X/825/2/98

Huang, C. X., Quinn, S. N., Vanderburg, A., et al. 2020, ApJL, 892, L7, doi: 10.3847/2041-8213/ab7302

Ida, S., & Lin, D. N. C. 2008, The Astrophysical Journal, 685, 584, doi: 10.1086/590401
Ida, S., & Lin, D. N. C. 2010, ApJ, 719, 810, doi: 10.1088/0004-637X/719/1/810
Ida, S., & Makino, J. 1992, Icarus, 96, 107, doi: https://doi.org/10.1016/0019-1035(92)90008-U
Iwasaki, K., & Ohtsuki, K. 2006, AJ, 131, 3093, doi: 10.1086/503606
Izidoro, A., Bitsch, B., Raymond, S. N., et al. 2021, A&A, 650, A152, doi: 10.1051/0004-6361/201935336
Izidoro, A., Ogihara, M., Raymond, S. N., et al. 2017, Monthly Notices of the Royal Astronomical Society, 470, 1750, doi: 10.1093/mnras/stx1232
Izidoro, A., Raymond, S. N., Morbidelli, A., Hersant, F., & Pierens, A. 2015, ApJL, 800, L22, doi: 10.1088/2041-8205/800/2/L22
Jayawardhana, R., Coffey, J., Scholz, A., Brandeker, A., & van Kerkwijk, M. H. 2006, ApJ, 648, 1206, doi: 10.1086/506171
Kokubo, E., & Ida, S. 1995, Icarus, 114, 247, doi: https://doi.org/10.1006/icar.1995.1059
—. 1998, Icarus, 131, 171, doi: https://doi.org/10.1006/icar.1997.5840
Kokubo, E., & Ida, S. 2000, Icarus, 143, 15, doi: 10.1006/icar.1999.6237
—. 2002, ApJ, 581, 666, doi: 10.1086/344105
Kolmogorov, A. N., & Morrison, N. 1950, Foundations of the theory of probability (Chelsea publ. Co)
Kominami, J., & Ida, S. 2004, Icarus, 167, 231, doi: 10.1016/j.icarus.2003.10.005
Korth, J., Chaturvedi, P., Parviainen, H., et al. 2024, The Astrophysical Journal Letters, 971, L28, doi: 10.3847/2041-8213/ad65fd
Lambrechts, M., & Johansen, A. 2012, A&A, 544, A32, doi: 10.1051/0004-6361/201219127
—. 2014, A&A, 572, A107, doi: 10.1051/0004-6361/201424343
Laughlin, G., Butler, R. P., Fischer, D. A., et al. 2005, ApJ, 622, 1182, doi: 10.1086/424686
Lee, E. J., & Chiang, E. 2015, ApJ, 811, 41, doi: 10.1088/0004-637X/811/1/41
Lee, E. J., Chiang, E., & Ormel, C. W. 2014, ApJ, 797, 95, doi: 10.1088/0004-637X/797/2/95
Lee, M. H., & Peale, S. J. 2002, ApJ, 567, 596, doi: 10.1086/338504
Lenz, C. T., Klahr, H., & Birnstiel, T. 2019, The Astrophysical Journal, 874, 36, doi: 10.3847/1538-4357/ab05d9
Levrard, B., Winisdoerffer, C., & Chabrier, G. 2009, ApJL, 692, L9, doi: 10.1088/0004-637X/692/1/L9
Li, J., Lai, D., Anderson, K. R., & Pu, B. 2020, Monthly Notices of the Royal Astronomical Society, 501, 1621, doi: 10.1093/mnras/staa3779
Li, J., Rodet, L., & Lai, D. 2024, MNRAS, 528, 1198, doi: 10.1093/mnras/stae045
Lin, D. N. C., Bodenheimer, P., & Richardson, D. C. 1996, Nature, 380, 606, doi: 10.1038/380606a0
Lin, D. N. C., & Papaloizou, J. 1986, ApJ, 309, 846, doi: 10.1086/164653
Lin, D. N. C., & Papaloizou, J. C. B. 1993, in Protostars and Planets III, ed. E. H. Levy & J. I. Lunine, 749
Lithwick, Y., & Wu, Y. 2014, Proceedings of the National Academy of Sciences, 111, 12610, doi: 10.1073/pnas.1308261110
Lu, T., Hernandez, D. M., & Rein, H. 2024, Monthly Notices of the Royal Astronomical Society, 533, 3708, doi: 10.1093/mnras/stae1982
Lu, T., Rein, H., Tamayo, D., et al. 2023, ApJ, 948, 41, doi: 10.3847/1538-4357/acc06d
Maciejewski, G., Golonka, J., Łoboda, W., et al. 2023, MNRAS, 525, L43, doi: 10.1093/mnrasl/slad078
MacLean, T., & Becker, J. 2025, ApJ, 987, 30, doi: 10.3847/1538-4357/add884
Marcy, G. W., Butler, R. P., Fischer, D. A., et al. 2002, ApJ, 581, 1375, doi: 10.1086/344298
Marzari, F., & Nagasawa, M. 2019, A&A, 625, A121, doi: 10.1051/0004-6361/201935065
Masset, F. S., Morbidelli, A., Crida, A., & Ferreira, J. 2006, The Astrophysical Journal, 642, 478, doi: 10.1086/500967
Matsumoto, Y., & Kokubo, E. 2017, AJ, 154, 27, doi: 10.3847/1538-3881/aa74c7
Matsumoto, Y., Nagasawa, M., & Ida, S. 2012, Icarus, 221, 624, doi: https://doi.org/10.1016/j.icarus.2012.08.032
Matsumura, S., Thommes, E. W., Chatterjee, S., & Rasio, F. A. 2010, The Astrophysical Journal, 714, 194, doi: 10.1088/0004-637X/714/1/194
McNeil, D. S., & Nelson, R. P. 2010, MNRAS, 401, 1691, doi: 10.1111/j.1365-2966.2009.15805.x
Millholland, S., & Laughlin, G. 2019, Nature Astronomy, 3, 424, doi: 10.1038/s41550-019-0701-7
Millholland, S., Laughlin, G., Teske, J., et al. 2018, VizieR Online Data Catalog, J/AJ/155/106
Millholland, S. C., He, M. Y., Ford, E. B., et al. 2021, AJ, 162, 166, doi: 10.3847/1538-3881/ac0f7a
Millholland, S. C., He, M. Y., & Zink, J. K. 2022, AJ, 164, 72, doi: 10.3847/1538-3881/ac7c67
Moorhead, A. V., & Adams, F. C. 2008, Icarus, 193, 475, doi: 10.1016/j.icarus.2007.07.009
Mulders, G. D., Pascucci, I., Apai, D., & Ciesla, F. J. 2018, AJ, 156, 24, doi: 10.3847/1538-3881/aac5ea

Mustill, A. J., Davies, M. B., & Johansen, A. 2015, ApJ, 808, 14, doi: 10.1088/0004-637X/808/1/14

Naoz, S. 2016, ARA&A, 54, 441, doi: 10.1146/annurev-astro-081915-023315

Ngo, H., Knutson, H. A., Hinkley, S., et al. 2016, ApJ, 827, 8, doi: 10.3847/0004-637X/827/1/8

Obertas, A., Van Laerhoven, C., & Tamayo, D. 2017, Icarus, 293, 52, doi: https://doi.org/10.1016/j.icarus.2017.04.010

Otegi, J. F., Bouchy, F., & Helled, R. 2020, A&A, 634, A43, doi: 10.1051/0004-6361/201936482

Paardekooper, S. J., & Mellema, G. 2004, A&A, 425, L9, doi: 10.1051/0004-6361:200400053

—. 2006, A&A, 453, 1129, doi: 10.1051/0004-6361:20054449

Pollack, J. B., Hubickyj, O., Bodenheimer, P., et al. 1996, Icarus, 124, 62, doi: 10.1006/icar.1996.0190

Press, W. H., Teukolsky, S. A., Vettering, W. T., & Flannery, B. P. 2003, European Journal of Physics, 24, 329–330, doi: 10.1088/0143-0807/24/3/701

Pu, B., & Lai, D. 2019, Monthly Notices of the Royal Astronomical Society, 488, 3568, doi: 10.1093/mnras/stz1817

—. 2021, Monthly Notices of the Royal Astronomical Society, 508, 597, doi: 10.1093/mnras/stab2504

Pu, B., & Wu, Y. 2015, ApJ, 807, 44, doi: 10.1088/0004-637X/807/1/44

Radzom, B. T., Dong, J., Rice, M., et al. 2025, The Astronomical Journal, 169, 189, doi: 10.3847/1538-3881/ad9dd5

Rafikov, R. R. 2002, ApJ, 572, 566, doi: 10.1086/340228

—. 2006, ApJ, 648, 666, doi: 10.1086/505695

Rasio, F. A., & Ford, E. B. 1996, Science, 274, 954. http://www.jstor.org/stable/2891291

Rasio, F. A., Tout, C. A., Lubow, S. H., & Livio, M. 1996, ApJ, 470, 1187, doi: 10.1086/177941

Raymond, S. N., Barnes, R., & Mandell, A. M. 2008, MNRAS, 384, 663, doi: 10.1111/j.1365-2966.2007.12712.x

Raymond, S. N., & Cossou, C. 2014, MNRAS, 440, L11, doi: 10.1093/mnrasl/slu011

Rein, H., & Liu, S. F. 2012, A&A, 537, A128, doi: 10.1051/0004-6361/201118085

Rein, H., & Spiegel, D. S. 2015, MNRAS, 446, 1424, doi: 10.1093/mnras/stu2164

Rein, H., & Tamayo, D. 2015, MNRAS, 452, 376, doi: 10.1093/mnras/stv1257

Ribas, Á., Bouy, H., & Merín, B. 2015, A&A, 576, A52, doi: 10.1051/0004-6361/201424846

Rice, M., Wang, S., & Laughlin, G. 2022, The Astrophysical Journal Letters, 926, L17, doi: 10.3847/2041-8213/ac502d

Rice, M., Wang, S., Wang, X.-Y., et al. 2022, AJ, 164, 104, doi: 10.3847/1538-3881/ac8153

Rivera, E. J., Laughlin, G., Butler, R. P., et al. 2010, ApJ, 719, 890, doi: 10.1088/0004-637X/719/1/890

Safronov, V. S. 1972, Evolution of the protoplanetary cloud and formation of the earth and planets.

Sanchis-Ojeda, R., Winn, J. N., Dai, F., et al. 2015, The Astrophysical Journal Letters, 812, L11, doi: 10.1088/2041-8205/812/1/L11

Santerne, A., Moutou, C., Tsantaki, M., et al. 2016, A&A, 587, A64, doi: 10.1051/0004-6361/201527329

Schlaufman, K. C., & Winn, J. N. 2016, ApJ, 825, 62, doi: 10.3847/0004-637X/825/1/62

Schlichting, H. E. 2014, ApJL, 795, L15, doi: 10.1088/2041-8205/795/1/L15

Scholz, F. W., & Stephens, M. A. 1987, Journal of the American Statistical Association, 82, 918. http://www.jstor.org/stable/2288805

Sha, L., Vanderburg, A. M., Huang, C. X., et al. 2023, MNRAS, doi: 10.1093/mnras/stad1666

Smirnov, N. 1939, Moscow University Mathematics Bulletin, 2, 3

Spalding, C., & Batygin, K. 2017, AJ, 154, 93, doi: 10.3847/1538-3881/aa8174

Steffen, J. H., Ragozzine, D., Fabrycky, D. C., et al. 2012, Proceedings of the National Academy of Sciences of the United States of America, 109, 7982, doi: 10.1073/pnas.1120970109

Stevenson, D. 1982, Planetary and Space Science, 30, 755, doi: https://doi.org/10.1016/0032-0633(82)90108-8

Tamayo, D., Rein, H., Shi, P., & Hernandez, D. M. 2020, MNRAS, 491, 2885, doi: 10.1093/mnras/stz2870

Tamayo, D., Cranmer, M., Hadden, S., et al. 2020, Proceedings of the National Academy of Sciences, 117, 18194, doi: 10.1073/pnas.2001258117

Terquem, C., & Papaloizou, J. C. B. 2007, ApJ, 654, 1110, doi: 10.1086/509497

Torres, G., Fressin, F., Batalha, N. M., et al. 2011, ApJ, 727, 24, doi: 10.1088/0004-637X/727/1/24

Volk, K., & Gladman, B. 2015, The Astrophysical Journal, 806, L26, doi: 10.1088/2041-8205/806/2/l26

Wang, X.-Y., Rice, M., Wang, S., et al. 2024, The Astrophysical Journal Letters, 973, L21, doi: 10.3847/2041-8213/ad7469

Ward, W. R. 1997, Icarus, 126, 261, doi: 10.1006/icar.1996.5647

Wasserstein, R. L., & Lazar, N. A. 2016, The American Statistician, 70, 129, doi: 10.1080/00031305.2016.1154108

Winn, J. N., Fabrycky, D., Albrecht, S., & Johnson, J. A. 2010, ApJL, 718, L145, doi: 10.1088/2041-8205/718/2/L145

Wu, D.-H., Rice, M., & Wang, S. 2023, AJ, 165, 171, doi: 10.3847/1538-3881/acbf3f

Wu, D.-H., Zhang, R. C., Zhou, J.-L., & Steffen, J. H. 2019, Monthly Notices of the Royal Astronomical Society, 484, 1538, doi: 10.1093/mnras/stz054

Wu, Y., & Lithwick, Y. 2011, The Astrophysical Journal, 735, 109, doi: 10.1088/0004-637x/735/2/109

Wu, Y., & Murray, N. 2003, The Astrophysical Journal, 589, 605, doi: 10.1086/374598

Xie, J.-W., Dong, S., Zhu, Z., et al. 2016, Proceedings of the National Academy of Science, 113, 11431, doi: 10.1073/pnas.1604692113

Yee, S. W., & Winn, J. N. 2023, The Astrophysical Journal Letters, 949, L21, doi: 10.3847/2041-8213/acd552

Zawadzki, B., Carrera, D., & Ford, E. B. 2021, MNRAS, 503, 1390, doi: 10.1093/mnras/stab603

Zhou, J.-L., Lin, D. N. C., & Sun, Y.-S. 2007, ApJ, 666, 423, doi: 10.1086/519918

Zhu, W., Petrovich, C., Wu, Y., Dong, S., & Xie, J. 2018, ApJ, 860, 101, doi: 10.3847/1538-4357/aac6d5

Zink, J. K., Christiansen, J. L., & Hansen, B. M. S. 2019, MNRAS, 483, 4479, doi: 10.1093/mnras/sty3463